Supporting Information

Multicomponent Donor-π-Acceptor Covalent Organic Framework as Nanoporous Cation-Selective Separator for Durable Aqueous Zinc Ion Batteries

*Ling Chen, Tiancun Liu, Xiao-Meng Lu, Weiwei Sun, Yang Wu, Yifan Zhang, Chao Yang, Yong Wang**

L. Chen, X.-M. Lu, Dr. W. W. Sun, Dr. Y. Wu, Dr. Y. F. Zhang, Dr. C. Yang, Prof. Y. Wang
Department of Chemical Engineering
School of Environmental and Chemical Engineering
Shanghai University
Shanghai 200444, People's Republic of China
E-mail: yongwang@shu.edu.cn

Dr. T. C. Liu
Institute of New Energy
School of Chemistry and Chemical Engineering
Shaoxing University,
Shaoxing 312000, People's Republic of China

Experimental Section

Materials: All regents commercially available were used without further purification. TTT and DTDA were provided by Jilin Chinese Academy of Sciences-Yanshen Technology Co., Ltd. Mesitylene and dioxane were supplied from Shanghai Aladdin Bio-Chem Technology Co., Ltd. Aqueous acetic acid, $MnSO_4•H_2O$ and $KMnO_4$ were supplied from Sinopharm Chemical Reagent Co., Ltd. Glass fiber (GF) was provided by Whatman.

Synthesis of TTT-DTDA COF: The TTT-DTDA COF was synthesized by a modified solvothermal condition[1]. A 10 mL Pyrex tube was loaded with 4,4',4''-(1,3,5-triazine-2,4,6-triyl)trianiline (TTT, 53 mg, 0.15 mmol), thieno[3,2-b]thiophene-2,5-dicarbaldehyde (DTDA, 44.5 mg, 0.225 mmol), 0.5 mL of mesitylene, 1 mL of dioxane and 0.25 mL of 6 M aqueous acetic acid. After ultrasonication for 1 min, the resulting mixture was degassed via 3 freeze-pump-thaw cycles. Then the tube was sealed under vacuum and heated at 120℃ for 3 days. A brown colored precipitate was collected by centrifugation, washed with anhydrous methanol and finally with anhydrous acetone. The collected powders were purified by Soxhlet treatment with methanol (12 h) at 90℃, and then dried at 100℃ for 2 hours to yield a brown colored TTT-DTDA COF powder.

Synthesis of GF@TTT-DTDA Separator: The COFs modified GF separator were achieved by vacuum filtration[2]. A certain amount (3, 5 and 7 mg) of TTT-DTDA was ground in a mortar for 15 mins and dispersed in 50 mL methanol. After ultrasonication for 10 minutes, the above suspension was dropped on the GF in the suction filter unit and the excess suspension was filtered out. Finally, the modified GF was rinsed 3 times with methanol and dried overnight under vacuum at 60℃. By changing the mass of TTT-DTDA (3, 5 and 7 mg), the prepared GF composite separators were named GF@TTT-DTDA-3, GF@TTT-DTDA (main product, 5 mg) and GF@TTT-DTDA-7, respectively. All GF and composite GF separators are pressed into a disc with a diameter of 16 mm.

Synthesis of MnO_2: 0.76 g $MnSO_4•H_2O$ and 0.47 g $KMnO_4$ were dissolved in 30 mL deionized water (DIW) respectively. Subsequently, these two solutions were mixed together and stirred for 15 min. Afterwards, the mixture was transferred into a 100 mL Teflon-lined autoclave and heated to 160 °C for 12 h. Finally, the collected product was centrifuged, washed with DIW, and dried in a vacuum oven at 80 °C.

Material Characterization: Scanning electron microscopy (SEM, Hitachi SU1510) with an energy dispersive X-ray spectroscopy (EDX) working at 10 kV was used to capture the surface morphologies of samples. The XRD patterns was putted into on a Rigaku D/max-2550 V running at 40 kV and 30 mA, employing Cu Ka radiation. For the powder samples, the FT-IR spectra were obtained by using Nicolet iS50 FT-IR instrument by the mode of transmission. Weight losses and thermal processes of samples were analyzed by a thermogravimetric analyzer with differential scanning calorimetry (TG/DSC, NETZSCH STA 449F5). The purging gas was N_2 at a flow rate of 20 mL·min^{-1} and the heating rate was 10 K·min^{-1}. In each test, about 10 mg of sample was detected from 20 to 1000℃. A specially designed cell composing of Zn foil, the selected separators, electrolyte and Cu mesh was assembled for the *in situ* FTIR measurement by the ATR mode. *In situ* optical images were conducted by Zeiss Smartzoom 5. The thickness of Zn foil was obtained from atomic force microscope (AFM, BRUKER Dimension icon).

Electrochemical Measurements: CR2032 coin cells with different separators (GF@TTT-DTDA or GF) were assembled in an atmospheric environment for the following test. 2 M $ZnSO_4$ dissolved in deionized water was selected as the electrolyte. The consumed amount of electrolyte was controlled at 80 μL per cell. Measurements of Zn-based asymmetric and symmetric cells were implemented at LAND-CT2001 battery test system from 1 to 20 mA cm^{-2}. For the full cell based on MnO_2 cathodes testing, blending a certainly mass of the MnO_2, acetylene black and PVDF at a weight of 7:2:1, and then coating on stainless steel. After vacuum drying the cathode materials at 60 °C for 6 h. In addition, aqueous solution of 2 M $ZnSO_4$ and 0.01 M $MnSO_4$ was chosen as the testing electrolyte. The full batteries performance studied at the different current density in the 0.9-1.8 V voltage window. Cyclic voltammetry (CV), chronoamperometry (CA) , linear sweep voltammetry (LSV) and Electrochemical impedance spectroscopy (EIS) curve were acquired by Electrochemical Workstation CHI706E (Shanghai Chenghua Instrument).

Computational details: The geometry optimization and electrostatic potential of COF were performed using Dmol3 code[3]. The generalized gradient approximation (GGA)[4] of PBE scheme[5] were employed. DFT-D approach[6] was applied to treat the weak van der Waals (vdW) interactions between COF atoms. Geometry optimization energy tolerance was set to 1.0×10^{-5} Ha/atom and the Self-consistent field (SCF) for controlling the electronic minimization algorithm was set to 1.0×10^{-6}. The force and displacement of ions convergence tolerance of 0.002 Ha/Å and 0.005 Å was used to ensure successful optimization.

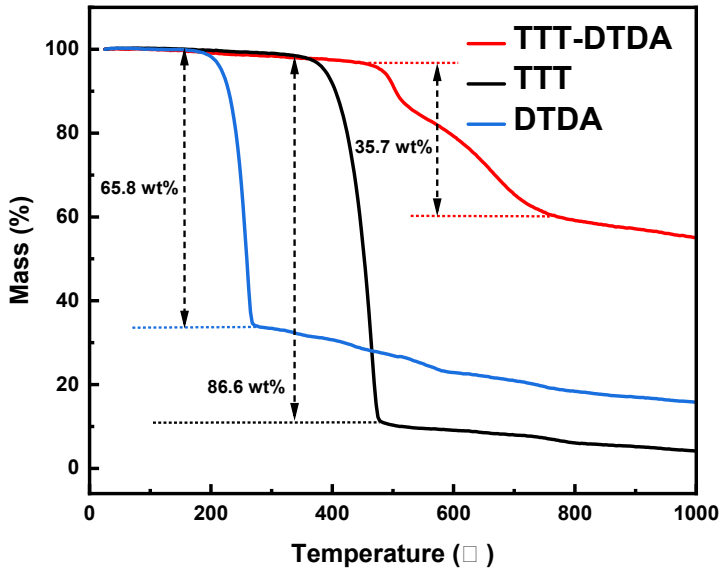

Figure S1. TGA curves of TTT, DTDA and TTT-DTDA COF. It can be found that TTT-DTDA can maintain stability at higher temperatures than monomer materials.

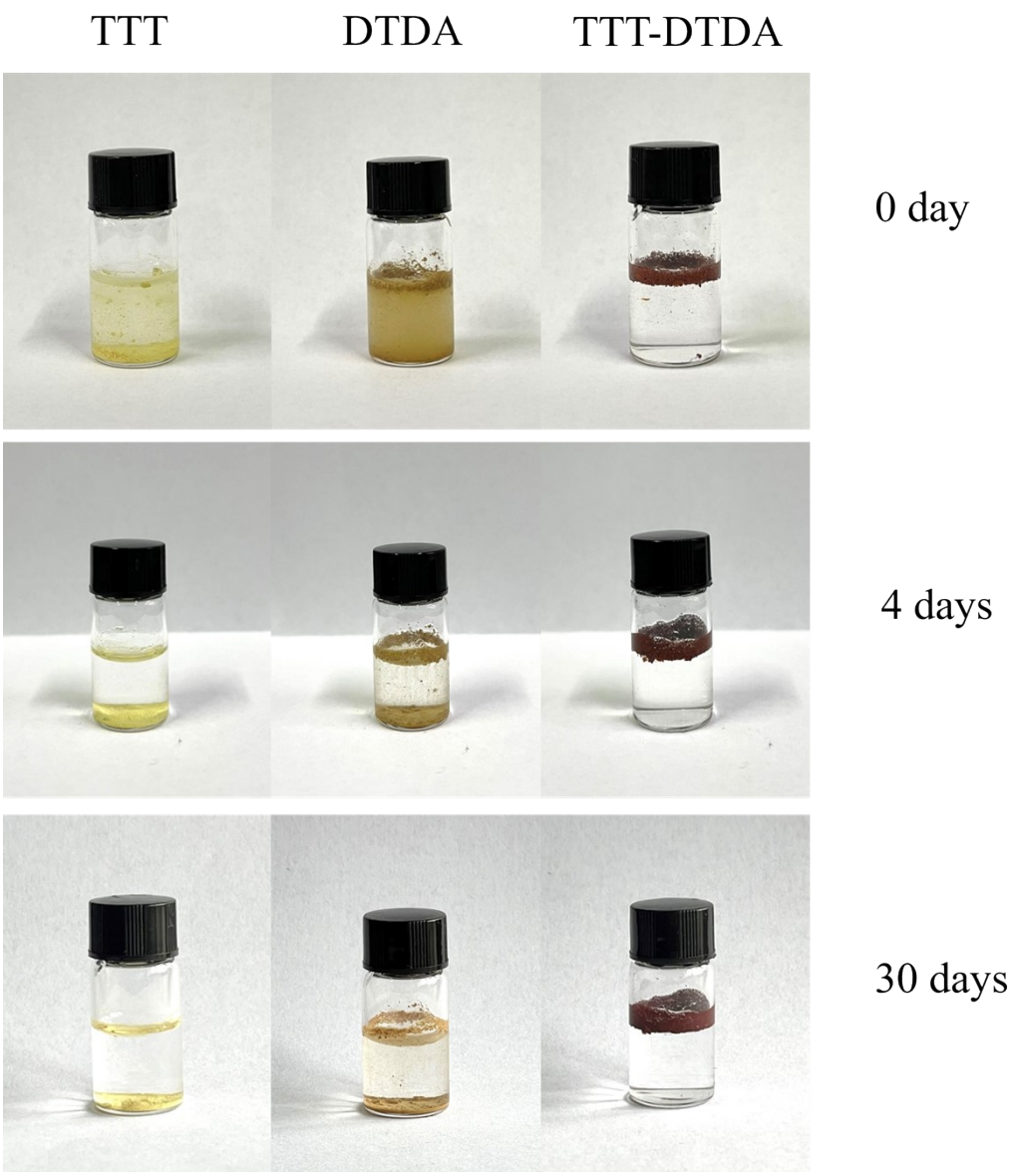

Figure S2. Photographs of TTT, DTDA and TTT-DTDA after immersing in the electrolyte for a period of time. Compared with small molecular monomers, TTT-DTDA has better stability in the electrolyte and is almost insoluble.

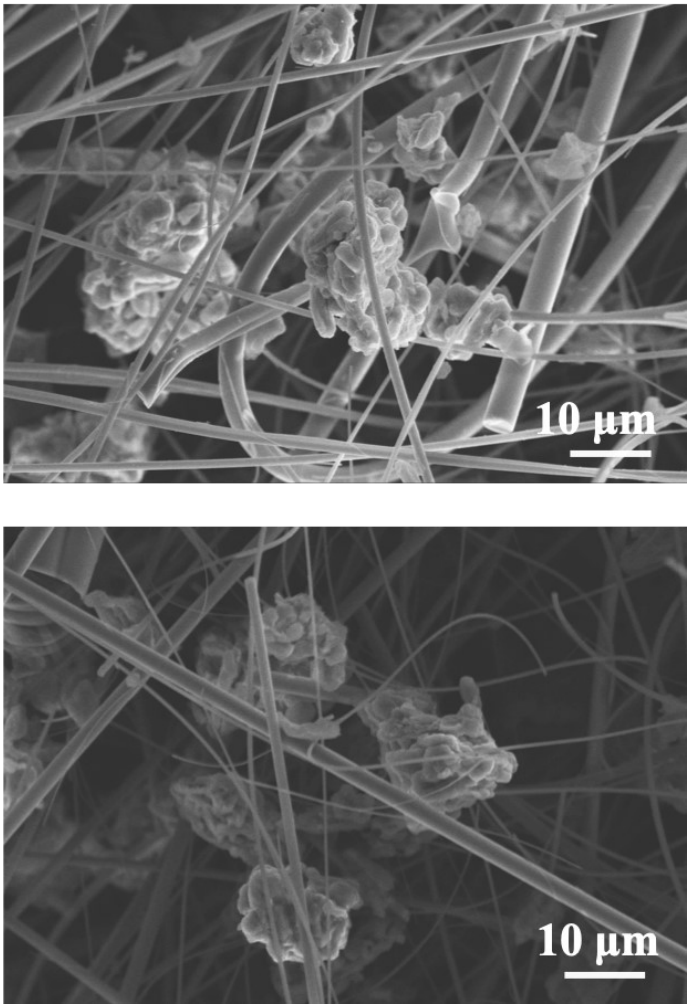

Figure S3. SEM images of GF@TTT-DTDA.

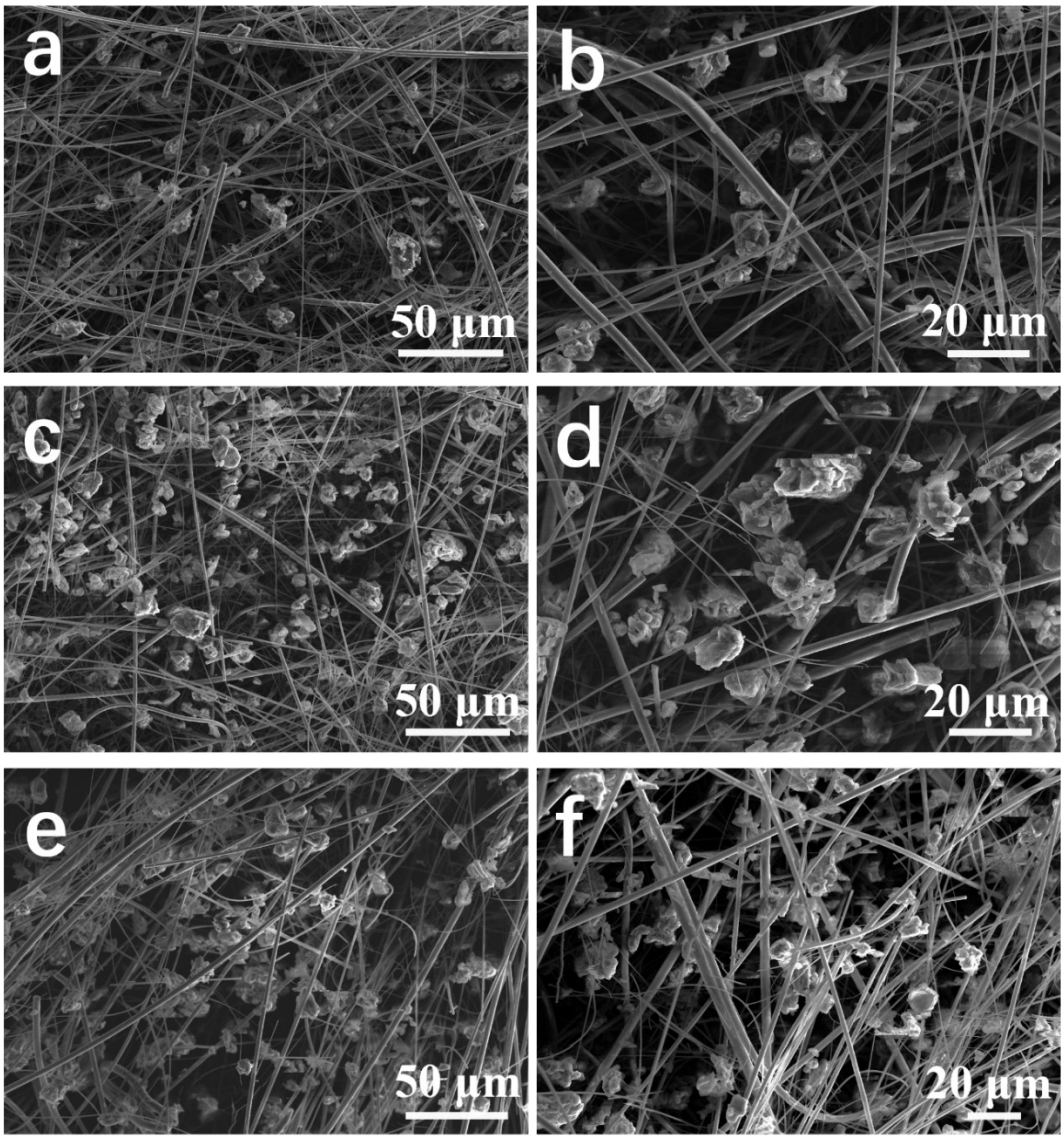

Figure S4. SEM images of (a, b) GF@TTT-DTDA-3, (c, d) GF@TTT-DTDA and (e, f) GF@TTT-DTDA-7. Compared with other loads, the GF@TTT-DTDA separator exhibits the most uniform and suitable distribution.

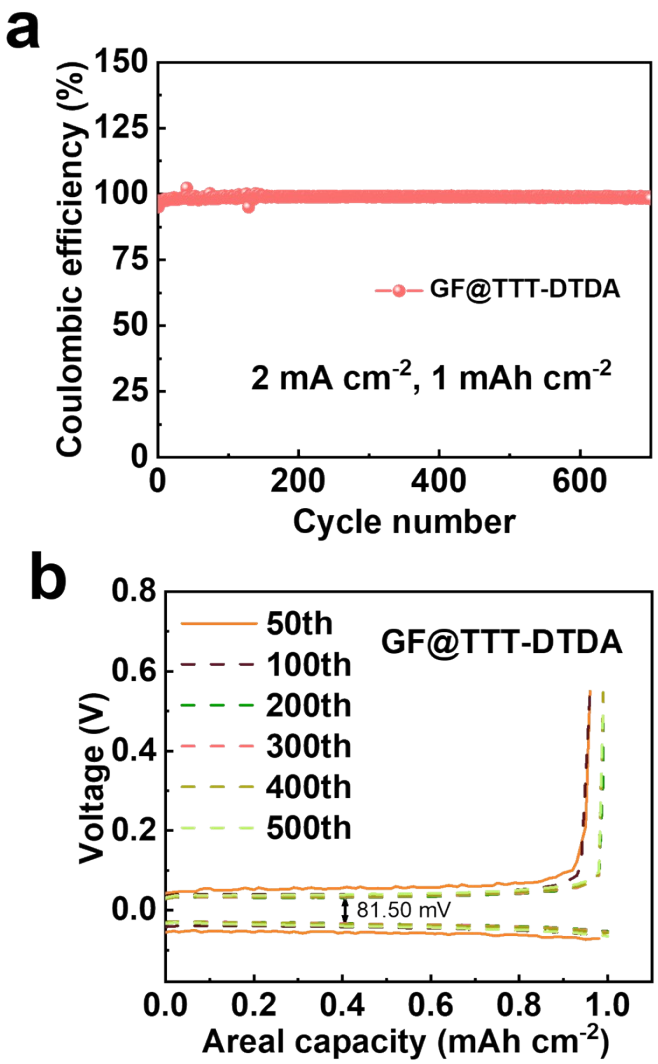

Figure S5. Electrochemical performances of GF@TTT-DTDA assembled half-cells at 2 mA cm^{-2},1 mA h cm^{-2}.

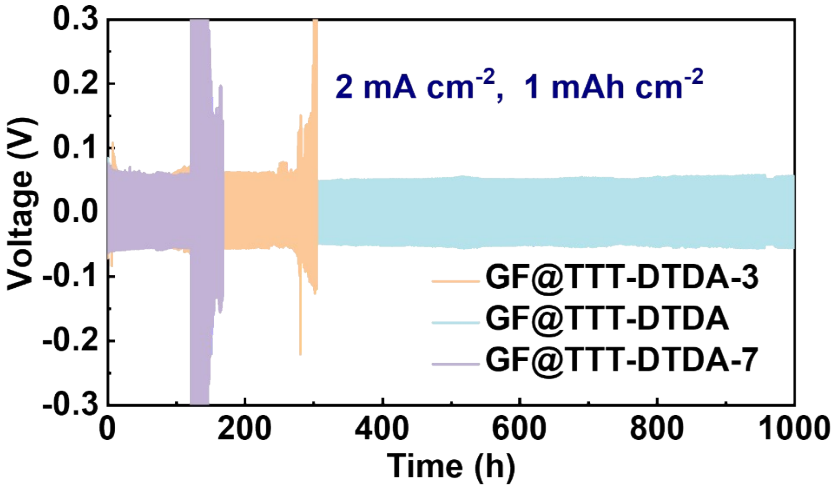

Figure S6. Voltage–time profiles of symmetric cells based on GF@TTT-DTDA-3, GF@TTT-DTDA and GF@TTT-DTDA -7 at 2 mA cm $^{-2}$, 1 mA h cm^{-2}.

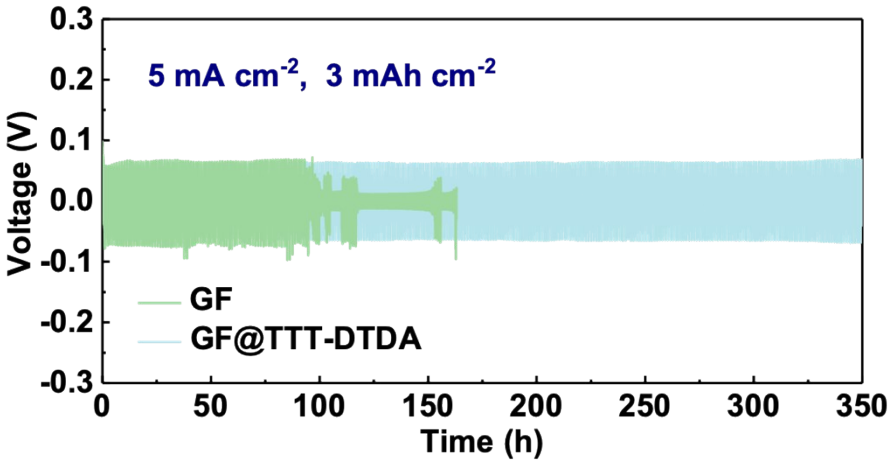

Figure S7. Cycling performance of symmetric cells with pristine GF and GF@TTT-DTDA at 5 mA cm^{-2}.

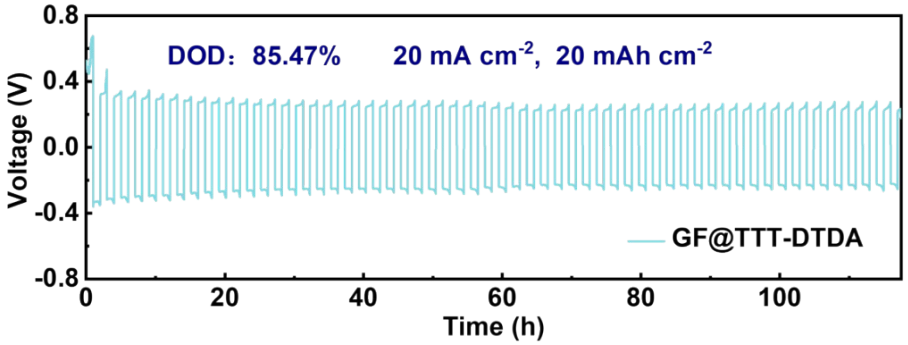

Figure S8. Cycling performance of symmetric cells with GF@TTT-DTDA at 20 mA cm^{-2} and 20 mAh cm^{-2}.

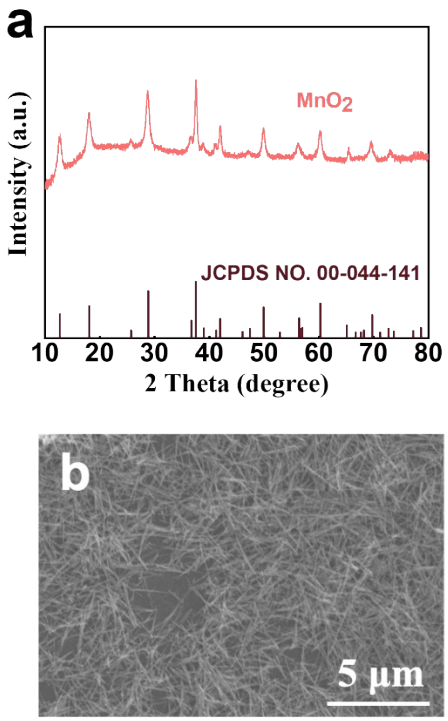

Figure S9. MnO_2 was synthesized and characterized: (a) XRD patterns and (b) SEM image.

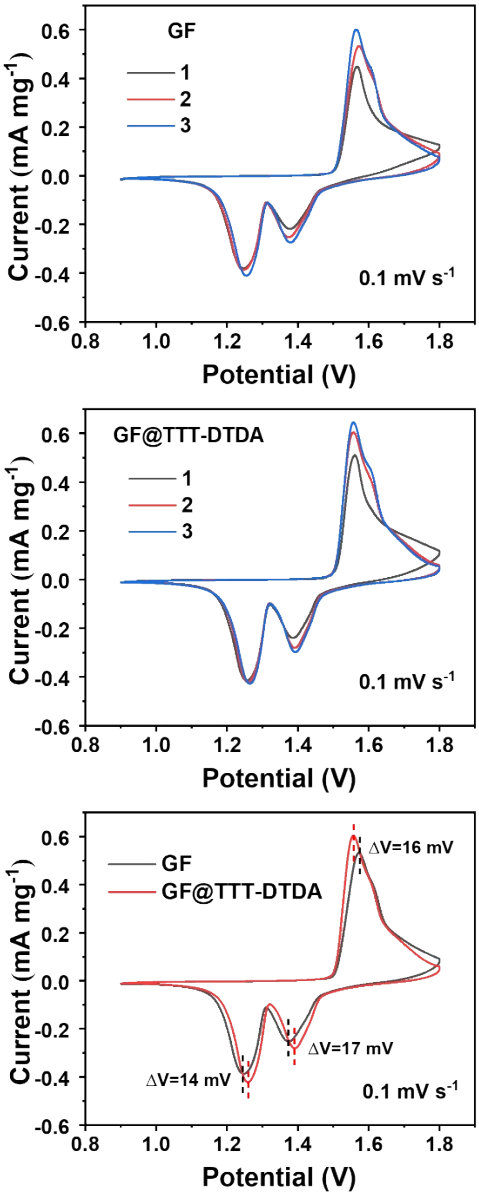

Figure S10. The CV curve was tested by assembling the cell with MnO_2 as the cathode and zinc foil as the anode. GF or GF@TTT-DTDA separator are used as separators respectively.

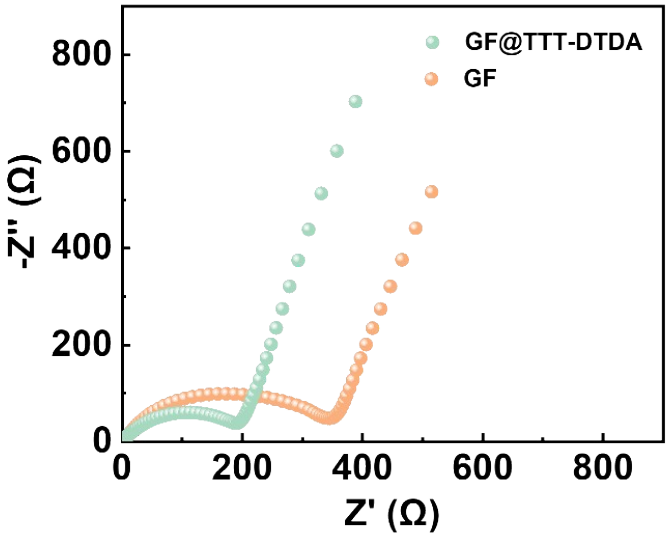

Figure S11. EIS curves of the full batteries.

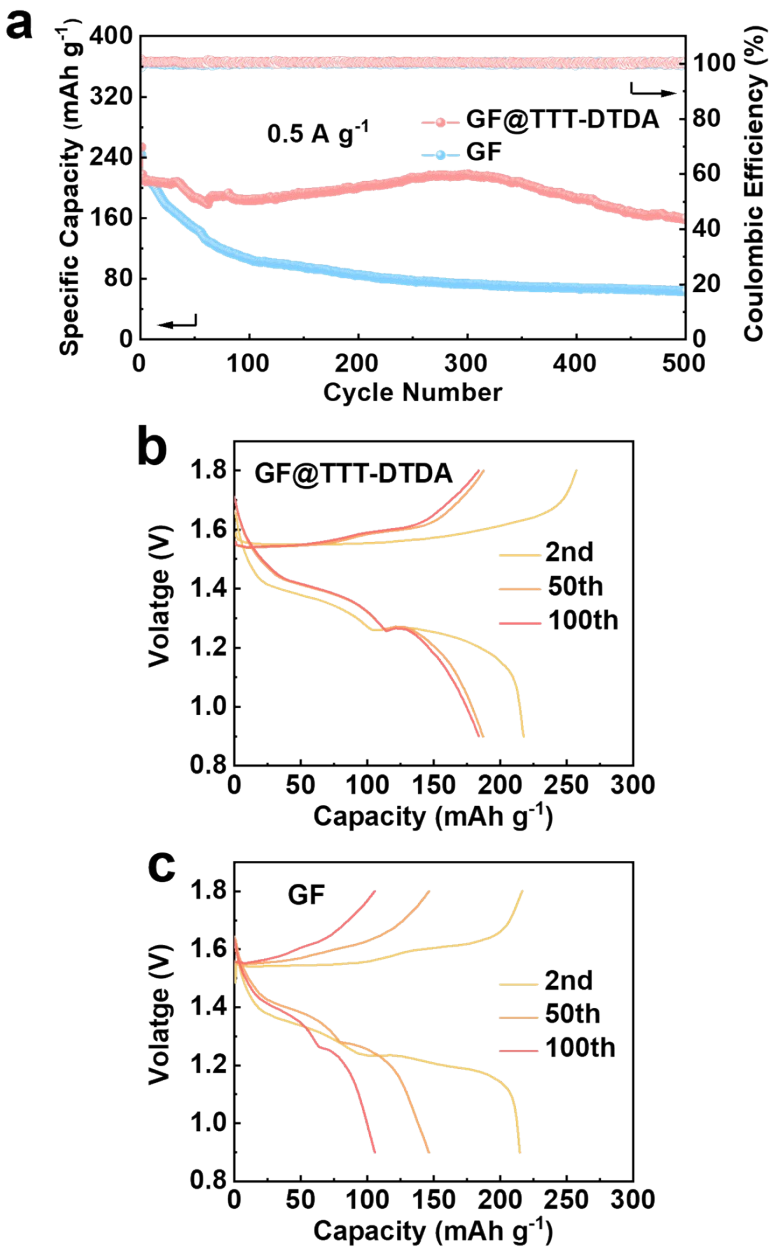

Figure S12. Electrochemical performances of Zn//MnO_2 full batteries at a current density of 0.5 A g^{-1}. (a) Long-term cycling performance. Voltage profiles of Zn//MnO_2 batteries using the (b) GF@TTT-DTDA and (c) GF separators under different cycles. The GF cell exhibited a fast and irreversible decline in its capacity during the initial 50 cycles, resulting in a specific capacity decrease to less than 40 mA h g^{-1}. After 500 cycles, the GF@TTT-DTDA battery retained over 160 mA h g^{-1} of capacity. The GF@TTT-DTDA full battery has a larger specific capacity than the GF full battery. Voltage polarization of GF@TTT-DTDA cells remains relatively constant from the 2nd to 50th cycles, while GF cells exhibit gradual polarization elevation due to zinc dendrite presence, leading to capacity decline.

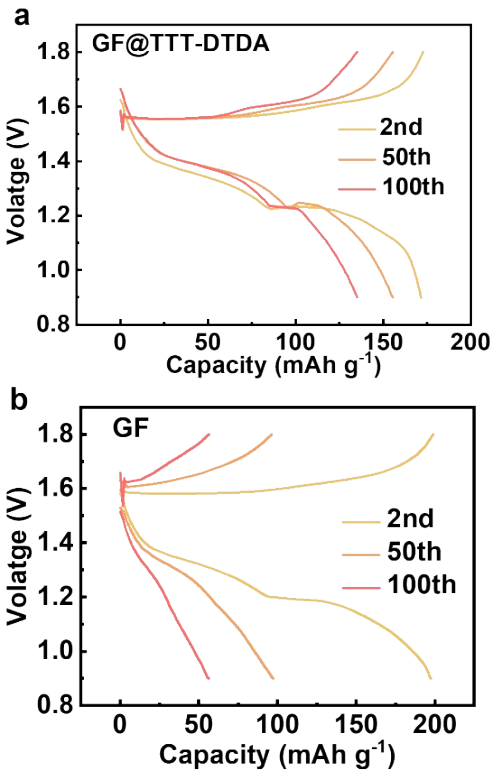

Figure S13. Voltage profiles of Zn//MnO_2 batteries using the (a) GF@TTT-DTDA and (b) GF separators under different cycles at 1 A g^{-1}.

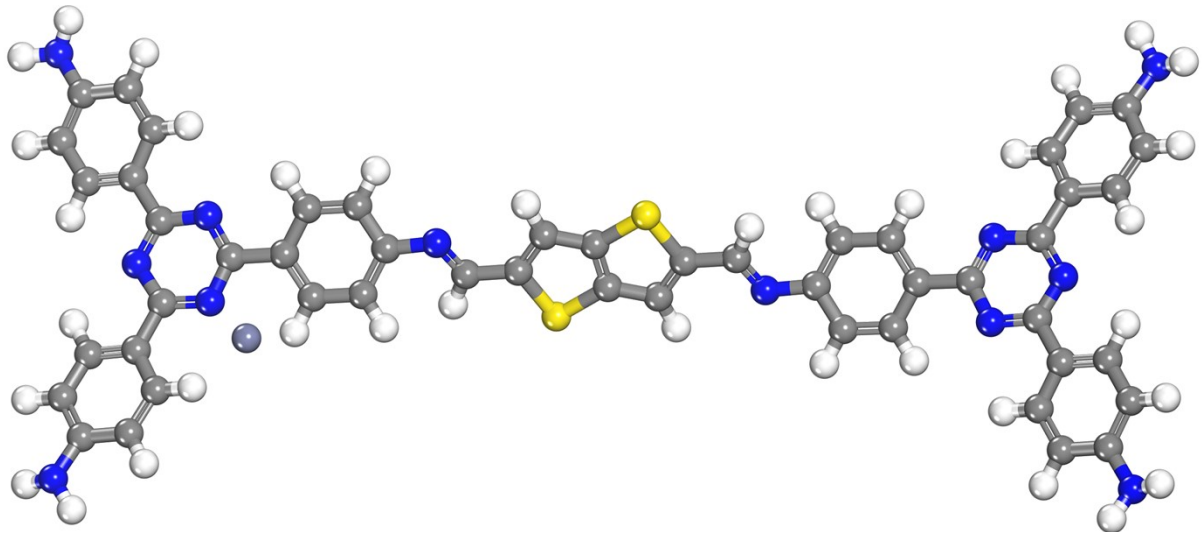

Figure S14. Simulation of the interaction between Zn ions and triazine ring (site 1) in the TTT-DTDA structure.

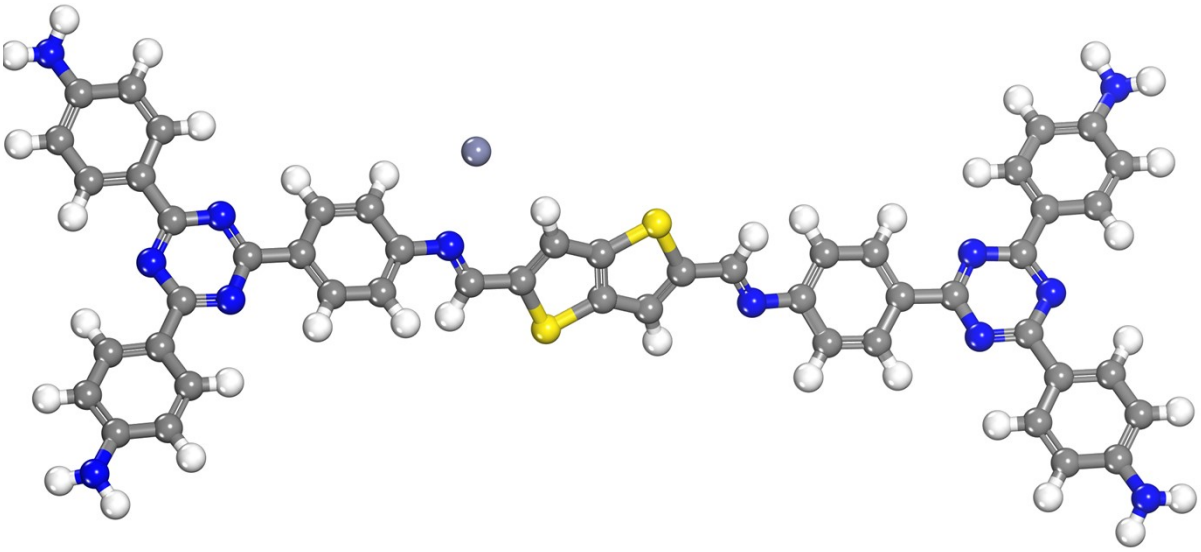

Figure S15. Simulation of the interaction between Zn ions and N site (site 2) in the TTT-DTDA structure.

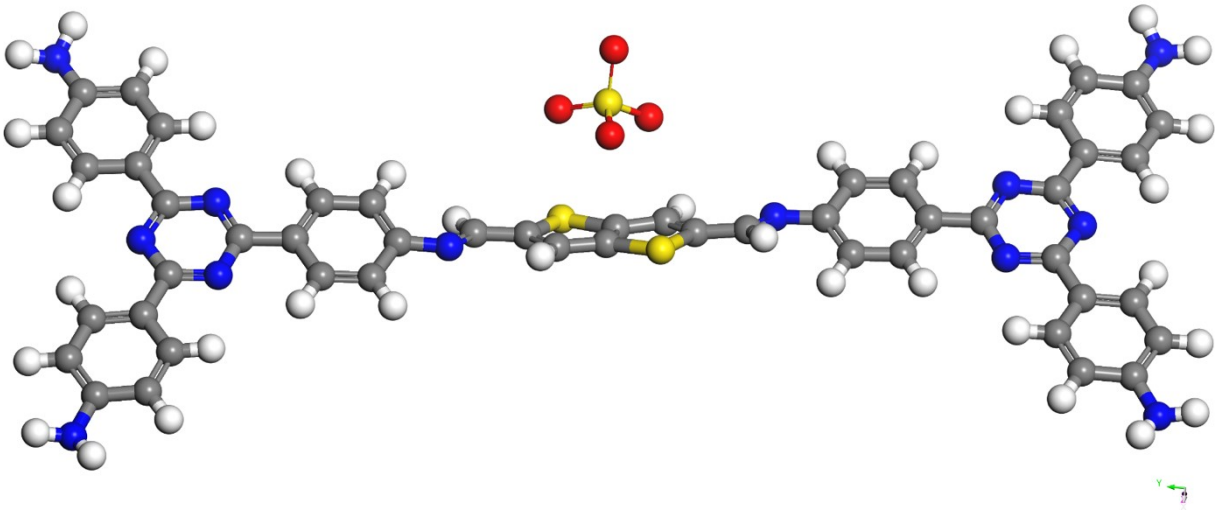

Figure S16. Simulation of the interaction between SO_4^{2-} and thieno[3,2-b]thiophene Units (site 3) in the TTT-DTDA structure.

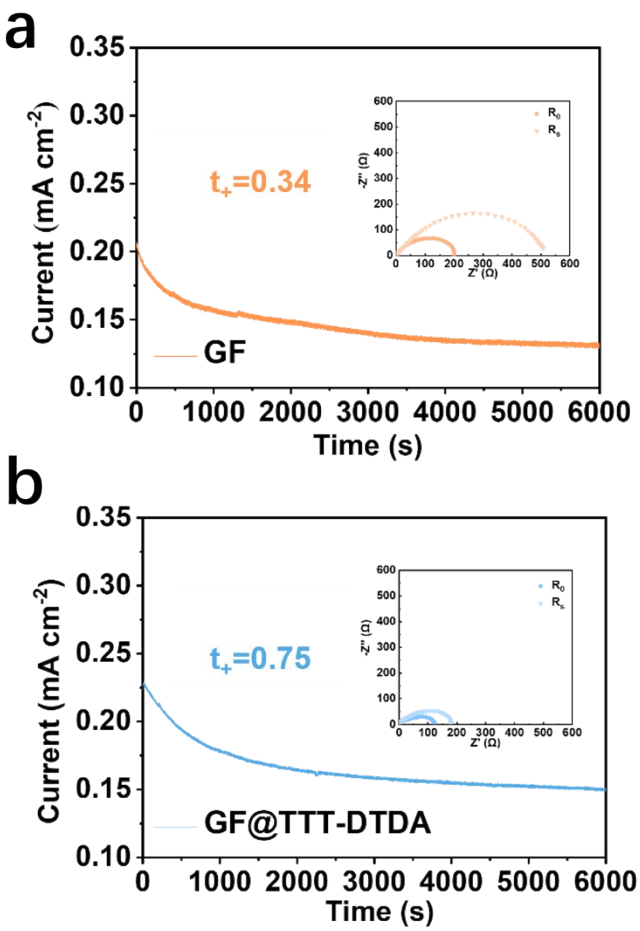

Figure S17. For (a) GF and (b) GF@TTT-DTDA based symmetric cells, the i-t curves and EIS spectra before and after polarization were tested, respectively.

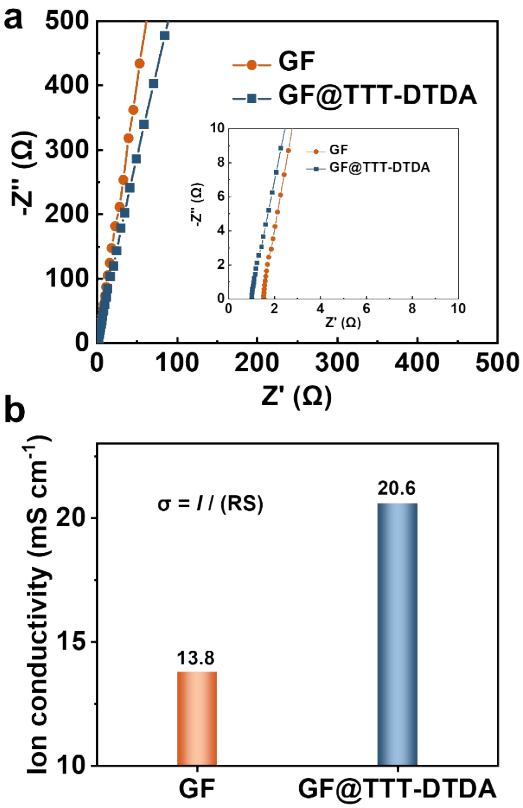

Figure S18. (a) Nyquist plots for GF and GF@TTT-DTDA separator were tested by assembling stainless steel symmetric batteries. The cell assembled by GF@TTT-DTDA exhibited a lower impedance value. (b) The calcualted ionic conductivities of GF and GF@TTT-DTDA separator.

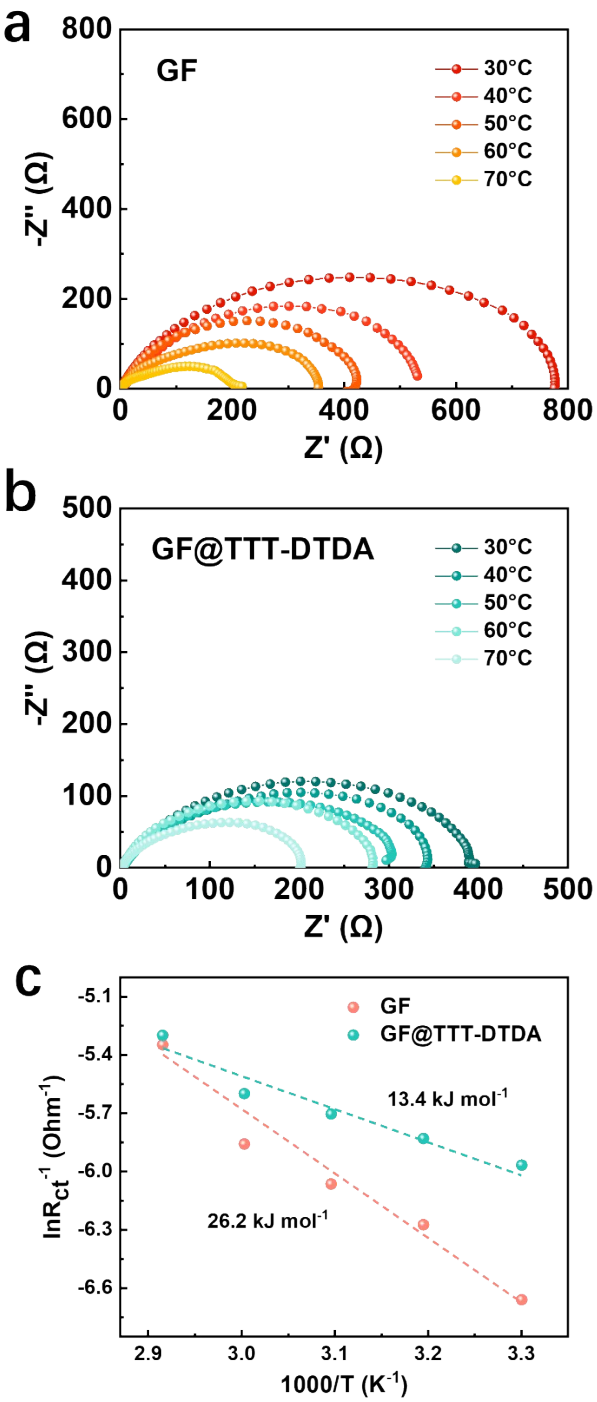

Figure S19. Nyquist plots of cells using the (a) GF and (b) GF@TTT-DTDA separators at different temperatures. (c) The calculated activation energy.

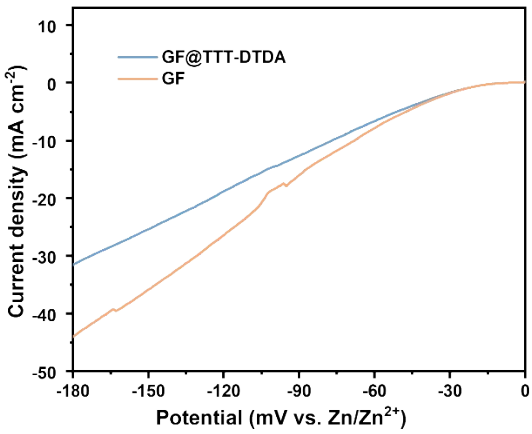

Figure S20. Linear sweep voltammetry curves of ZnllTi batteries with GF and GF@TTT-DTDA at a scan rate of 0.1 mV s^{-1}.

Table S1. Performance comparison with previous zinc metal batteries using various separators.

Materials	C/CD. [mA (h) cm^{-2}]	Life [h]	OP. [mV]	Reference
TTT-DTDA	1/1	1240	48	**This work**
	2/1	1000	50	
	5/3	350	52	
CNF-SO_3Zn	1/0.5	500		*Adv. Funct. Mater.* 2022, 32, 2200429
MZn-60	0.2/0.2	800	47	*Angew. Chem. Int. Ed.* 2021, 60, 2861 – 2865
Nafion	5/0.5	553	~100	*J. Mater. Chem. A* 2021, 9, 4734–4743
CT@NZF@N	0.5/0.5	300	~80	*J. Power Sources* 2023, 553, 232321
TTA-DHTPA-COF@GF@Gr	5/5	600		*J. Power Sources 2024, 608, 234658*
	10/10	200		
TTA-DHTPA-COF@GF	5/5	80		
Zn-BTC membrane	2/2	700	~100	*Adv. Mater.* 2020, 32, 2004240
	5/2.5	350	125	

	1/3	250	~110	
g-C_3N_4 coated separator	5/1	320	~160	Chem. Eng. J. 2022, 433, 134077
	3/1	590	130	
CT separator	1/0.5	1200	~80	*ACS Sustainable Chem. Eng.* 2022, 10, 8350−8359
	2/4	700	~50	
PBC@CF	1/0.5	322	~50	*Electrochim. Acta* 2022, 430, 141129
	2/1	<100	~50	
Janus separator	0.5/0.25	500	75	*Nano-Micro Lett.* 2021, 13, 73
	2/1	500	89	

Note: Current/ Capacity density (C/CD); Overpotential (OP).

References

1 P. Pachfule, A. Acharjya, J. Roeser, R. P. Sivasankaran, M.-Y. Ye, A. Brückner, J. Schmidt, A. Thomas, *Chem. Sci.* **2019**, 10, 8316.

2 J. Liu, J. Zhang, J. Zhu, R. Zhao, Y. Zhang, Y. Ma, C. Li, H. Zhang, Y. Chen, *Nano Res.* **2023**, 16, 12601.

3 B. Delley, *The Journal of Chemical Physics* **1990**, 92, 508.

4 J. P. Perdew, K. Burke, M. Ernzerhof, *Phys. Rev. Lett.* **1996**, 77, 3865.

5 D. Vanderbilt, *Physical Review B* **1990**, 41, 7892.

6 A. Tkatchenko, M. Scheffler, *Phys. Rev. Lett.* **2009**, 102, 073005.